Biophysical Journal Volume 65 November 1993 2068–2077

Simulated Formation of Polymer Domains in Sickle Hemoglobin

Qun Dou and Frank A. Ferrone
Department of Physics and Atmospheric Science, Drexel University, Philadelphia, Pennsylvania 19104 USA

ABSTRACT Using experimentally observed processes of linear growth, heterogeneous nucleation, and polymer bending, with no additional assumptions, we have been able to model the two-dimensional formation of polymer domains by sickle hemoglobin. The domains begin with twofold symmetry and proceed toward closure into spherulites at a constant rate. Relationships derived from the simulations presented and the requirements of scaling result in simple expressions for the sensitivity of the closure times to the model input parameters and allow the results to be extended to regions not actually simulated. For concentrations above approximately 25 g/dl, closure times are longer than the time required for the conclusion of the polymerization reaction, and thus incomplete spherulites will be the dominant geometry at high concentrations. Moreover, spherulites are not predicted to form in times less than a few seconds, implying that spherulites will not form during the transit of erythrocytes through the capillaries. Polymer-polymer exclusion, surface nucleation, and monomer exhaustion were also explored and found to have only weak effects on the results.

INTRODUCTION

Sickle hemoglobin (HbS) differs from HbA by the presence of a neutral valine on the surface of the molecule, where a negatively charged glutamic acid is normally found ($\beta 6$). The result of this mutation is that deoxygenated HbS molecules at sufficiently high concentrations can assemble into long, 14-strand polymers. Polymers form by two types of nucleation processes (Ferrone et al., 1980, 1985a). Heterogeneous nucleation entails creation of a new polymer by nucleation on the surface of another polymer and has been directly observed. Homogeneous nucleation entails the nucleation of a new polymer from monomer association in solution. While the latter has not been directly observed, there is strong evidence for such a process in the dramatic stochastic fluctuations that occur in the first polymer formation process. Since polymers created by heterogeneous nucleation are attached to others, a polymer network is the natural outcome of this double nucleation mechanism. Although polymers can be broken from one another (when placed on electron-microscopy grids, for example (Briehl et al., 1990)), this has not been observed in solutions which are not sheared (Samuel et al., 1990). At long times these networks, or polymer domains, assume a spherulitic from in which polymers radiate uniformly in all directions (Beach et al., 1988; Hofrichter, 1986; Mickols et al., 1988; White and Heagan, 1970). At early times, such radial structures are not observed. Lower symmetry patterns, sometimes referred to as "wheat sheaves" have been observed directly by optical microscopy (White and Heagan, 1970). Evolution of twofold to radial symmetry has been seen in birefringence measurements (Basak et al., 1988). There is clearly a connection between the double nucleation mechanism and spherulitic domains, but a detailed mechanism for domain formation has not been demonstrated.

The direct observations of the heterogeneous process by Briehl and coworkers set the stage for an attempt to model the formation of domains (Samuel et al., 1990). Prior to that work, parallel growth of the new fiber with respect to the old was tacitly assumed (Ferrone et al., 1985a), but alternatives, such as growth of the new polymer at an angle to the originating fiber, could not be ruled out. Since the bulk theories previously developed (Ferrone et al., 1985a) did not use the nucleation geometry in any significant way, they did not depend on geometrical assumptions and of course did not admit of any tests of the those assumptions. Briehl and workers also observed that the growing polymers are flexible, so that the heterogeneously nucleated fibers grow parallel for some distance after which they are deflected from the original direction. This allows splaying of the ends, and could ultimately permit the filling of a given spatial region. Without such an experimental fact, domain geometry is fixed by the nucleation geometry. However, it is unclear a priori whether it is possible for such a mechanism to form spherulites without additional assumptions.

The first goal of this paper is to see to what extent domain formation can be described by the present understanding of polymerization as discussed above in the absence of additional assumptions. The central facts to be described are the initial twofold symmetry which spreads to radial symmetry and the overall exponential growth.

The second goal of this work is to delineate the relationship between parameters that give rise to a spherulitic domain. Since domain structure begins in twofold symmetry, we wish to investigate if there are situations in which radial symmetry will not be assumed. We would like to understand the scaling behavior of the process, so that a limited set of simulations can be applied to a variety of conditions.

The spatial dependence in domain formation also creates additional complications in attempts to construct models for

Received for publication 24 May 1993 and in final form 10 August 1993.

Address reprint requests to Frank A. Ferrone at the Department of Physics and Atmospheric Science, College of Arts and Sciences, Drexel University, 32nd and Chestnut Streets, Philadelphia, PA 19104.

0006-3495/93/11/2068/10 $2.00

domain growth. Monomer diffusion is one such complication, which exists as the result of a monomer gradient, due in turn to the gradient of polymer density (Cho and Ferrone, 1990, 1991; Zhou and Ferrone, 1990). Monomers will diffuse into regions in which the formation of polymers has diminished the initial monomer concentration. This diffusion increases the total concentration of hemoglobin at the center of domains, and may mean that polymer crowding effects influence domain growth even at early stages of the overall reaction. Such effects have been seen in our previously employed radial growth models and have been demonstrated in subsequent experiments. Hence the effects of a density ceiling must be explored in any attempt to study domain formation.

Understanding domain formation is an important step in connecting the microscopic polymer formation process with the macroscopic vasooclusive events which characterize sickle cell disease. For example, it has been hypothesized that domain number and geometry can play a role in the pathophysiology (Ferrone, 1989).

We report here simulations of domain formation in two dimensions. We find that a twofold wheat sheaf pattern is readily generated, which broadens toward forming a full spherulite. Bent sheaf patterns which resemble sickle cell morphology are also generated naturally. Spreading of the pattern is assisted by imposing a ceiling or cutting off nucleation. The number of monomers incorporated grows approximately exponentially, in accord with observations. Spherical symmetry is assumed slowly however, and the results of these simulations suggest that rapidly formed samples with multiple homogeneous nucleation sites might not form recognizable domains before monomer concentration is lowered to the solubility.

METHODS

Basic numerical methods and assumptions

The calculation begins with the formation of a nucleus from which one polymer grows. New polymers are generated on the surface of the existing ones, corresponding to the heterogeneous nucleation in the double nucleation model. Polymer growth is linear, with randomly distributed deflection points corresponding to the bending of the polymer; this is independent of the original polymer. The detailed structure of the HbS polymers is neglected. Polymers are treated as straight lines of zero thickness that elongate at a constant rate, j. Growth is confined to two dimensions, though the polymers are assumed to be flexible enough to cross each other. In the simulation, a fiber does not move once in place. Hence the polymer ends migrate only by growth.

The elongation rate, j, is taken to be the experimental value of 0.11 μm/s, which was measured at a concentration of 12.8 mM (heme) and a temperature of 28°C (Samuel et al., 1990). The step size of growth is set at 210 nm, which is the diameter of the 14-strand HbS fiber. The choice of step size and the growth rate determined the time resolution of the simulation to be 0.19 s. The elongation rate j is proportional to the net monomer addition rate, J. Given a 14-strand fiber, the average elongation is 0.46 nm per added monomer, i.e., $j = 0.46\text{ nm} \times J$.

Polymer deflection occurs by changing the direction of growth. The polymers that are to undergo deflection are chosen randomly. The average number of deflection events per unit time is determined by the number of polymer ends times an adjustable parameter, b, which will be referred to as the deflection rate. The total number of deflection events in each step of simulation are made to follow a Poisson distribution. The angles of the deflected polymer are uniformly distributed between zero and a maximum angle. In all results reported here, the maximum angle is 0.4 radian. Bending of this magnitude has been observed by Samuel et al. (1990). A somewhat more realistic approach would have been to use a Gaussian distribution of angles, but this would have significantly slowed the simulations with little gain in accuracy.

The number of nucleation events is determined similarly by a nucleation rate multiplied by the total number of monomers in the polymer. This is the same as the mechanism used by Ferrone et al. (1985a) in which the rate of nucleation is taken as being proportional to the total concentration of polymerized monomers. The newly formed nuclei are placed randomly on the existing polymers. and the polymers grown from these nuclei are parallel to the ones on which the nucleation occurs.

The heterogeneous nucleation rate, g, ranged from 6×10^{-9} to 6×10^{-6} nucleations per monomer per second, while deflection rates range from 0.02 to 0.32 deflections per polymer per second. At $g = 6 \times 10^{-9}$ the total polymerized monomers N increase at a constant rate, $d \ln N/dt$ that matches that measured in experiment (after a brief initial linear phase discussed below) (Ferrone et al., 1985b). A deflection rate of 0.08 s^{-1} gives an average straight polymer segment of about 1.38 μm.

Monomer diffusion has been predicted (Zhou and Ferrone, 1990) and observed (Cho and Ferrone, 1990, 1991) in polymer domains. For the simulations performed here, diffusion will be fast enough to keep the monomer concentration close to its initial value. Thus, diffusion does not explicitly appear, even though it is implicitly included to avoid the difficulty tracking the decrease in monomer concentration.

The simulations were carried out on a Apple Macintosh MacIIfx computer with 8 M of memory. The code is written in Pascal, and is available from the authors.

Analytic considerations

The outcome of the simulations depends on three parameters, g, J, and b. However, the parameters are connected by a scaling relation. If the parameters are each increased by a factor σ, the result is equivalent to decreasing the time step by the factor σ without any change. If s is the distribution of polymers, $s(\sigma g, \sigma J, \sigma b, t) = s(g, J, b, t/\sigma)$. This follows from the fact that g, J, and b are rates, and as such involve a change in some parameter per unit time step. However, the computation involves iteration steps, whose meaning is realized by assigning a time to each step. If the steps are σ times shorter, the reactions are all σ times faster.

If the total number of polymerized monomers is given as N, and the number of polymers is N_p, then the net equations can be written quite simply. Polymers are formed by a nucleation rate times the number of monomers already in polymers. Thus

$$dN_p/dt = g\,N. \tag{1}$$

Monomers add to both ends of a polymer at a rate J, and thus

$$dN/dt = 2JN_p. \tag{2}$$

In molecular terms, the net monomer addition rate J is given by

$$J = k_+ \gamma c - k_-, \tag{3}$$

where k_+ and k_- are the microscopic rate constants for monomer addition and loss, respectively, c is the concentration of solution monomers, and γ is an activity coefficient, which will in general depend on c. There is no decrease in concentration because diffusion is assumed rapid enough to keep the monomer concentration fixed. Both ends are assumed to elongate at the same rate, in agreement with observations (Samuel et al., 1990).

The solution for N from Eqs. 1 and 2 is

$$N = N_0 \cosh Bt + N_{po} \frac{B}{g} \sinh Bt, \tag{4}$$

in which N_0 is the number of monomers at $t = 0$ and N_{po} is the number of polymers at $t = 0$. B is the exponential growth rate, and is given by

$$B = \sqrt{2Jg}. \quad (5)$$

This solution becomes exponential for $Bt > 1$. We take $N_{po} = 1$ and $N_0 = 46$, the latter being the number of monomers in a segment whose length is equal to its diameter. This is somewhat arbitrary, but its choice has little effect in the following simulations. The total number of polymerized monomers is independent of the bending rate.

Extensions to the Model

When polymers grow closely parallel to each other to form a bundle, only the surface of the bundle can act as the site of heterogeneous nucleation, while the inside of the bundle is made inactive. In that case the number of nucleation events should be proportional to the total surface area of the polymers. At the same time, a polymer can not grow into a region where the polymer density is already high. These effects were not included in the basic simulation. Thus our results tend to overestimate B with a given nucleation rate, or equivalently, with a given B, the nucleation rate used in the simulation should be the lower limit of real g.

An approximation based on a spatial grid is used to study how crowding and surface nucleation will influence the results. If all monomers in a grid belong to one bundle, the the surface area S due to those monomers is proportional to $\sqrt{LN}$ where N is the number of monomers in the grid and L is the length of the cell. Therefore the average number of nucleation events per unit time is given by a nucleation rate times the square root of the number of monomers in a particular grid, summed over all grids. The errors of this approximation come from the facts that there may more bundles than one in a particular cell and L is not a constant but depends on the angle of the fibers. These errors should decrease with the size of the grid. Likewise, to include the effects of crowding, we imposed a ceiling on the elements of the grid, so that nucleation and growth would cease in that grid element when the density exceeded a certain value. The grid size used for both nucleation and crowding effects was 0.2×0.2 μm. The major conclusions of this work do not critically depend on the choice of nucleation methods.

RESULTS OF SIMULATIONS

Simulations were performed using $g = 6 \times 10^{-6}$, 6×10^{-7}, 6×10^{-8}, and 6×10^{-9} s^{-1}, and $b = 0.02$, 0.08, and 0.32 s^{-1}, respectively, for each of the preceding values of g, while j is fixed at 0.11 μm/s. All simulations are stopped when the number of polymer segments, defined as the straight polymer between deflection points or ends, reaches 1000. Higher nucleation rates lead to shorter running time, thus smaller domain size when the simulations finishes. There are about 10^6 monomers polymerized in a simulation.

Fig. 1 shows the results of a typical simulation. As can be seen, the domain expands and spreads in width. Because of the random curvature, the patterns are generally skewed to one side or the other. Memory limitations prevented us from following the domain till full radial structure is reached. However, nothing indicated failure of the extrapolations, and indeed extrapolation from shorter times to times actually observed would be quite accurate.

Visual inspection shows that the resulting patterns are characteristically shaped like an "x," with two opposite quadrants filled with polymers and the other two empty. The center of the cross usually has the highest density. Exceptions to this observation are those with $g = 6 \times 10^{-9}$, whose patterns do not show a distinct center. This is most likely due to the fact that the simulation is not carried out long enough. (Simulations with larger values of g likewise were ill-defined at their earliest times.) We also note that some of the patterns show a curvature which makes them curiously similar to the shape of sickled red blood cells (Fig. 2).

Fig. 3 shows the total number of monomers included in polymers as a function of time for three different sets of

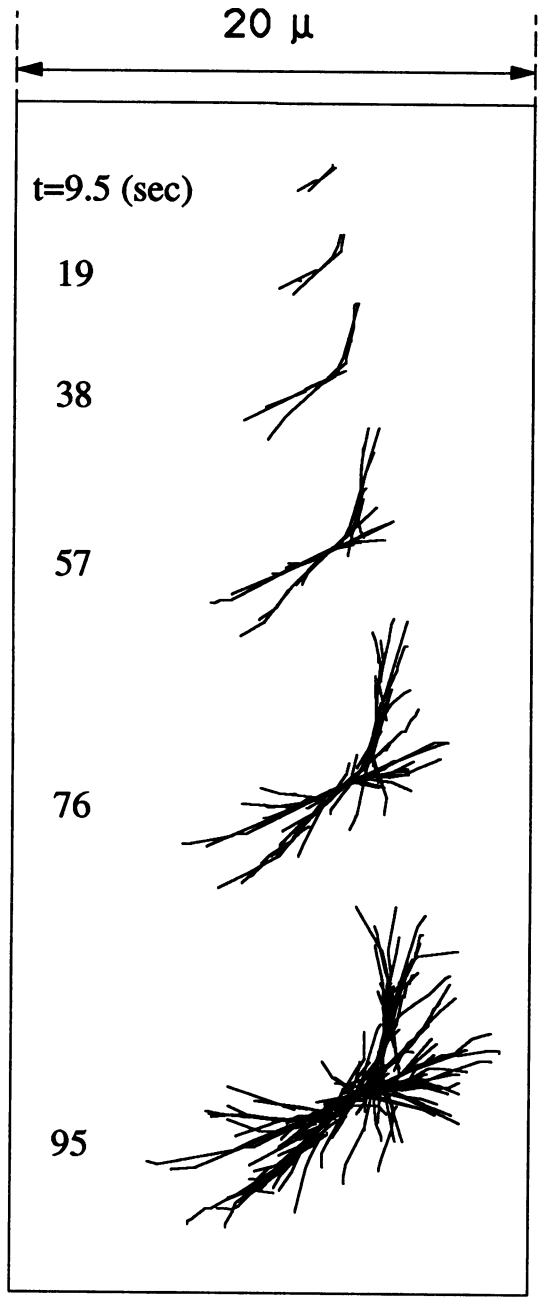

FIGURE 1 Typical results of two-dimensional simulation. $b = 0.08$ deflections per polymer per sec; $g = 6 \times 10^{-6}$ nucleation events per incorporated monomer per second, and $j = 0.11$ μm/s. As can be seen, the domain grows longer and wider. Because of the random curvature of the polymers, the patterns are generally skewed to one side or the other. The number of monomers polymerized in a typical simulation is about 10^6.

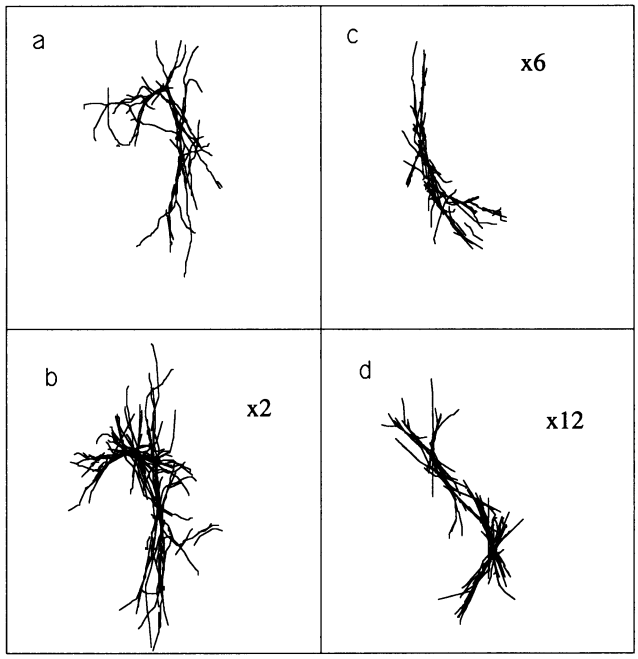

FIGURE 2 In a number of cases, a "sickle" form spontaneously appears. Four different examples are shown. Because of different growth rates, the sizes are different, and the magnifications are therefore indicated relative to the domain in the upper left, which is in a box that measures 350 μm on a side. The following parameters were employed: (*a*) $b = 0.02\ s^{-1}$, $g = 6 \times 10^{-9}\ s^{-1}$; (*b*) $b = 0.02\ s^{-1}$, $g = 6 \times 10^{-8}\ s^{-1}$; (*c*) $b = 0.08\ s^{-1}$, $g = 6 \times 10^{-7}\ s^{-1}$; (*d*) $b = 0.08\ s^{-1}$, $g = 6 \times 10^{-6}\ s^{-1}$. For all cases, $j = 0.11\ \mu$m/s.

parameters. 30 simulations begun with different random seeds have been averaged for each set of conditions. As can be seen, the increase can be described accurately by Eq. 4 and is exponential at later times.

In a given simulation, the time taken for N to reach a certain value varies noticeably due to the stochastic nature of nucleation and deflection processes. Fig. 4 *a* shows the variation of time to reach a specific N.

A central issue in the simulation is the widening of the domain as it assumes a radial structure. This was analyzed by treating the location of monomers in polymers as a density distribution. The maximum density point was taken as a reference and the distribution between two concentric rings centered on the reference point was divided into 64 angular slices. The standard deviation of the angular density distributions was calculated, and its value, normalized over the total density, is used to represent the width of the domain, and hereafter called domain width, w. The radius of the outer ring is the maximum span of the domain, while the inner radius is 0.1 times the outer radius. The purpose of the inner ring is to exclude the center portion of the distribution which gives large angles but is irrelevant to the width of the domain. Furthermore, since a domain often consists of two unequal halves, each half is treated separately using the previously described method. The two halves are defined by drawing a line through the domain center perpendicular to the original direction of the first polymer. The average of the two standard deviations is defined as the domain width, and is used in the analysis. Fig. 5 illustrates the procedure as applied to a typical domain.

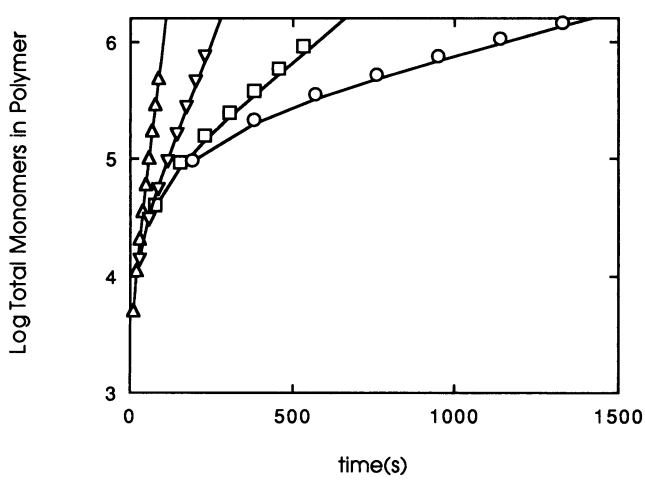

FIGURE 3 Total number of monomers included in polymers as a function of time, for $b = 0.08\ s^{-1}$; $j = 0.11\ \mu$m/s; $g = 6 \times 10^{-6}, 6 \times 10^{-7}, 6 \times 10^{-8}, 6 \times 10^{-8}\ s^{-1}$. The data average 30 runs each. As can be seen, the increase is close to exponential, and is very well fit by the lines, which are the solutions given by Eq. 4.

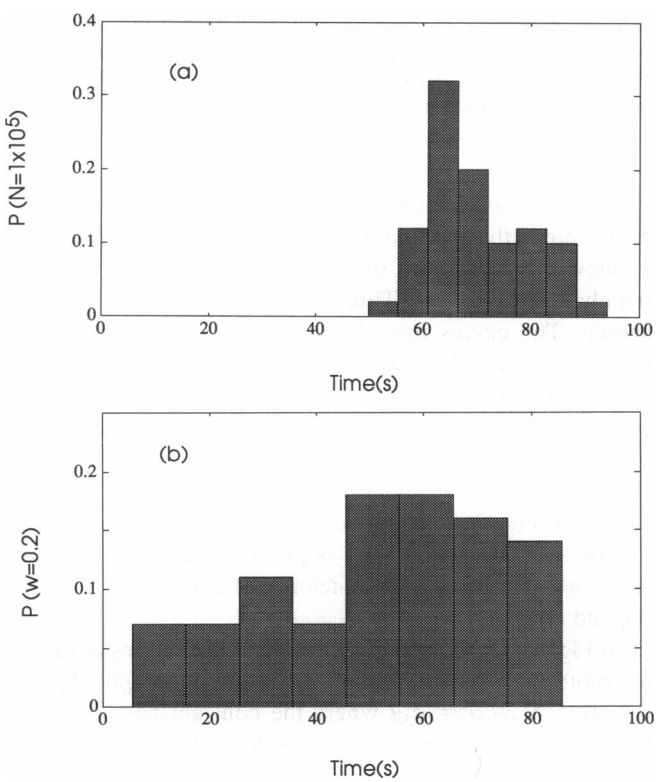

FIGURE 4 (*a*) Distribution of a time required to reach 10^5 monomers. $b = 0.08\ s^{-1}$, $g = 6 \times 10^{-6}\ s^{-1}$; $j = 0.11\ \mu$m/s. The histogram is normalized to unity; 30 curves have been run. Variation is due to the variability of heterogeneous nucleation. (*b*) Distribution of times for the polymer angular distribution to reach a width of 0.2 rad. Again the distribution of 30 curves is normalized to 1. The variation is due to the different bending which the polymers undergo.

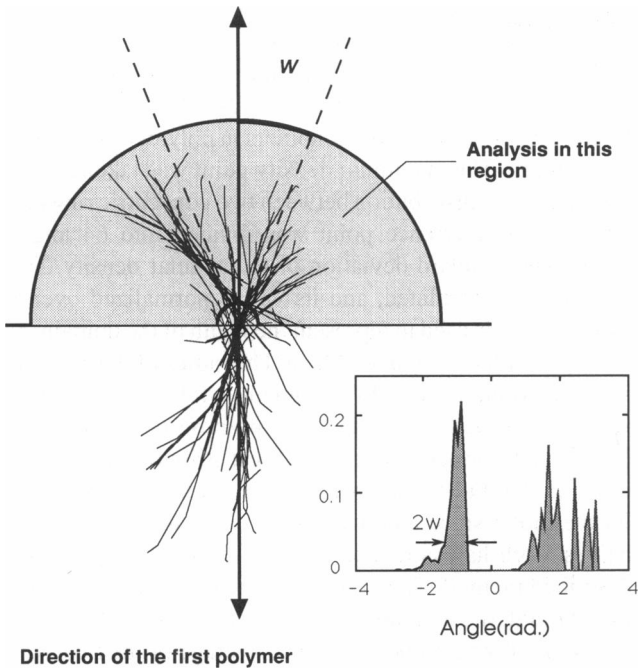

FIGURE 5 Analysis of polymer densities distribution. The maximum density point was taken as a reference and the distribution between two concentric rings centered on the reference point is divided into 64 angular slices. The standard deviation of the angular density distributions was calculated. Its value, normalized over the total density, is denoted w. The radius of the outer ring is the maximum span of the domain; the inner radius is 0.1 times the outer radius. The inner ring excludes large angles from the center portion of the distribution which are irrelevant to the width of the domain. Each half is treated separately, with the average of the two standard deviations defined as the domain width. The inset shows a density distribution for the polymers which have been drawn in the picture.

Fig. 6 shows the widening of the distribution of monomers. The width of the distribution, again averaged for 30 domains, is shown as a function of time. The widening is approximately linear in time. Three different deflection rates are shown. The curves have been fit with straight lines constrained to pass through the origin, i.e., $w = vt$. There is considerable fluctuation in the width at a given time. Fig. 4 *b* shows a histogram of the time to reach a given width for a series of simulations.

The square of v, the slopes of the lines in Fig. 6, is shown in Fig. 7 as a function of the deflection rate b. As can be seen, the square of v is proportional to the bending rate, i.e., $v^2 = ub$. The parameter u, of course, can and will depend on g and J.

In Fig. 8, the squares of u, which are the slopes in Fig. 7, are plotted against nucleation rate g, and once again display linearity. Now $u^2 = a_J g$ where the constant has been subscripted to indicate that it will only depend on J. Thus, combining the above observations, we have

$$v = (a_J g)^{1/4} b^{1/2}. \tag{6}$$

The constant a_J can be written as

$$a_J = a' J^{\beta}, \tag{7}$$

where β is a power to be determined. It is clear that this

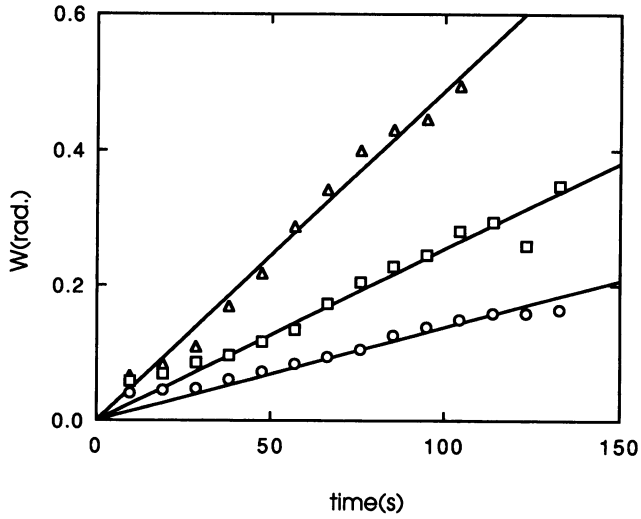

FIGURE 6 Widening of the distribution of monomers for various deflection rates. The width of the distribution, averaged for 30 domains, is shown as a function of time. The widening is approximately linear in time. Three different deflection rates are shown: $b = 0.02, 0.08, 0.32\ s^{-1}$ (*circles*, *triangles*, and *squares*, respectively). The curves have been fit with straight lines constrained to pass through the origin. For all three, $g = 6 \times 10^{-6}\ s^{-1}$ and $j = 0.11\ \mu m/s$.

equation must describe the form of the J dependence from the scaling relationships. Since v is a rate it must obey the scaling relationship described above, namely,

$$v(\sigma g, \sigma J, \sigma b) = \sigma v(g, J, b). \tag{8}$$

As written, Eq. 6 does not obey this rule unless a_J has the form of Eq. 7 with $\beta = 1$. Combining this with the definition of the exponential rate B from Eq. 5, and defining $a^4 = a'/2$, gives

$$v = a\sqrt{Bb}, \tag{9}$$

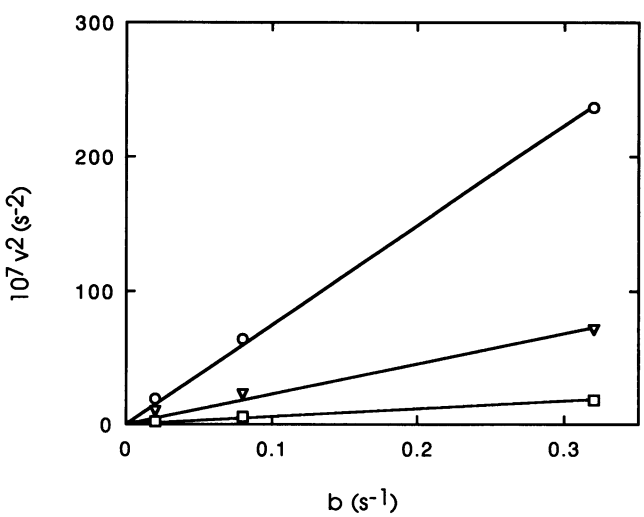

FIGURE 7 Widening rate v squared for three different deflection rates b as a function of the deflection rate. The slope of this curve is called u. The growth rate is calculated as the slope of the lines in Fig. 6.

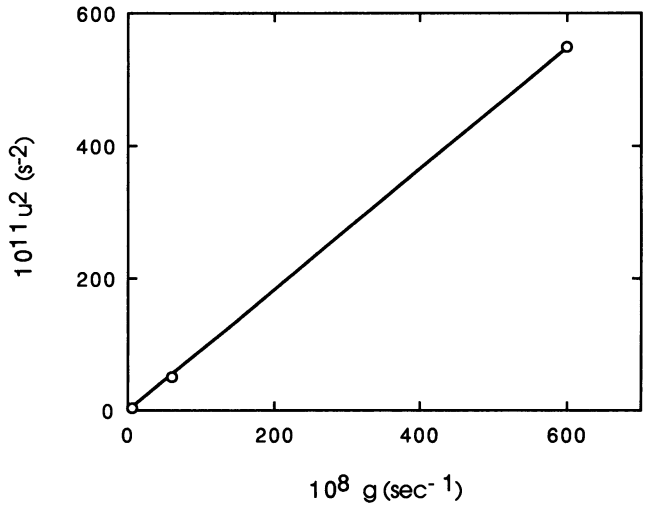

FIGURE 8 The squares of the slopes, u, in Fig. 7, for three nucleation rates g, are plotted as a function of g.

in which a is a constant which cannot depend on b, g, or J. Note that in this description, v, the rate of domain widening, does not explicitly depend on the polymer growth rate J. Both B and b are readily measurable parameters.

Extensions to the basic model

Changing the method of nucleation to the "square root" rule produced very similar patterns. The growth of polymer is still exponential, as shown in Fig. 9 *a* although slightly slower at longer times than that predicted by Eq. 5. The linear relationship between w and t still holds. (Fig. 9 *b*).

We next turn to the effects of terminating nucleation. This simulation was done as a crude way of examining the sensitivity to changing rates of nucleation, as might be seen as the monomer population was exhausted. Since nucleation is highly sensitive to concentration, the physical situation which corresponds to this simulation requires that the nucleation rate would be more abruptly decreased than the growth rate as the pool of free monomers decreases. Shutting off nucleation had a very small effect on the spread of the width as a function of time.

Fig. 10 *a* shows the outcome of a simulation with nucleation shut off as described above. Clearly, the growth of the total of polymerized molecules becomes much slower (linear in time when nucleation terminates). Fig. 10 *b* shows that there is also a change in the rate of domain expansion, albeit a smaller change than is seen in the monomer incorporation. It is interesting to consider the width as a function of the number of monomers. Shutting off nucleation effectively *widens* the domain in this representation. Fewer polymerized monomers are required for the same width of the domain. Or, for each monomer added to the domain, the domain will widen more if the monomer is added via growth rather than by nucleation.

Finally we looked at the effect of imposing a ceiling on the concentration of monomers in polymers, as a representation

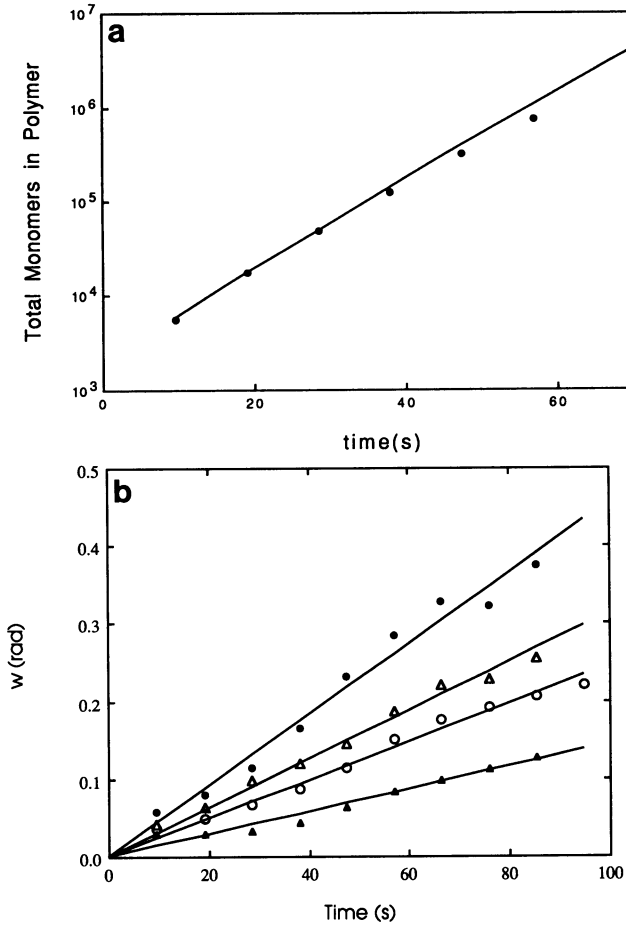

FIGURE 9 Results using a discrete grid to simulate surface nucleation. (*a*) The total number of monomers is compared with the analytic equation (*solid line*) from Eq. 4, which does not account for finite polymer width. The agreement is quite good until the last decade, where the differences are not more than a factor of 2. (b) Growth of the width as a function of time is still linear as in Fig. 6. Four different values of b are shown, 0.02, 0.07, 0.14, and 0.28. $g = 2.4 \times 10^5$ and $j = 0.11$ μm/s.

of crowding effects. Fig. 11 *b* shows that the increase in domain width is insensitive to the effects of crowding, while Fig. 11 *a* shows that the total concentration increases more slowly. As observed in the simulation above, in which nucleation is terminated, the width is also greater for a given number of monomers in which dense regions saturate than it was when nucleation and growth continued unabated.

DISCUSSION

By incorporating the experimentally observed polymer bending into the double nucleation description of polymerization, it is possible to describe the transformation of a single fiber into wheat-sheaf bundles and then to spherulitic domains. No such process appears in bulk descriptions, and yet this is critical in deciding what the final spatial distribution of polymers will be. While the spreading into a domain is easily anticipated without the foregoing calculations, several features are not expected, and the quantitative features, especially the concentrations at which closure does not occur, can

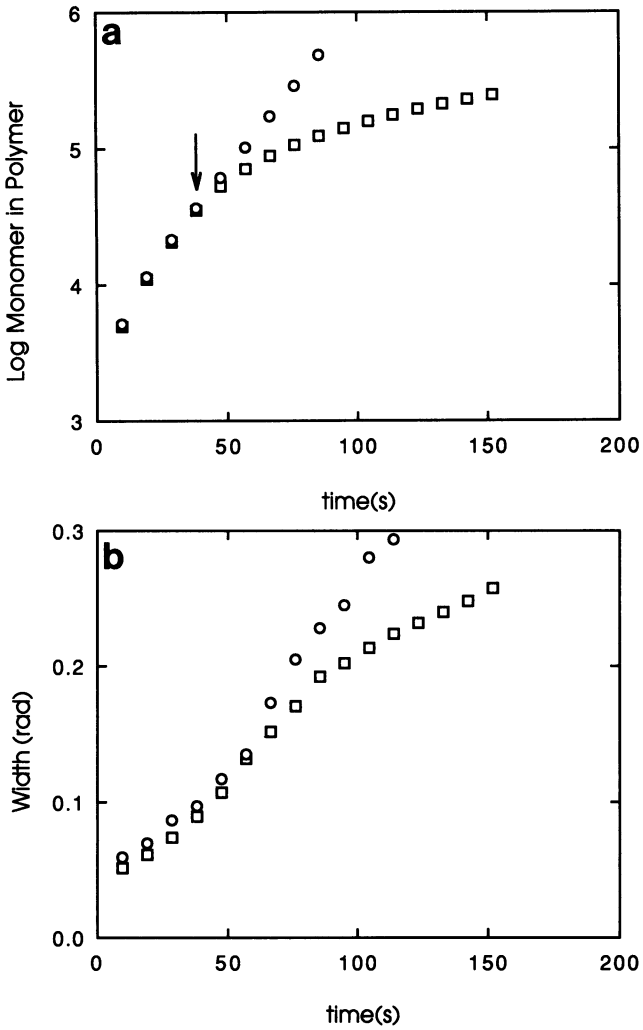

FIGURE 10 Simulation with an abrupt termination of nucleation. The arrow drawn at the fourth point shows the last point at which nucleation occurred. (*a*) The total number of monomers polymerized increases only linearly once nucleation ceases. (*b*) Domain widening also slows; however, the width for a given number of monomers is greater here than without termination.

arise only from the detailed simulation and scaling calculations. Particularly unexpected results are the simple description of the rate of domain spreading, and the lack of sensitivity of the spreading of the domain width to effects such as the termination of nucleation or the imposition of a low ceiling of polymer crowding. In the sections that follow, the results are compared with experimental data, and a number of implications are discussed.

Domain closure

From the linear rate of widening of the domain, it is clear that the domain will close and its shape become radial if it grows for a long enough time. It is possible, though, that the supply of available monomers may be exhausted before the domain is closed. When the width = $\pi/2$, the domain can be regarded as closed. A closure time T_c is given as

$$T_c = \frac{\pi}{2v} = \frac{2^{1/4}\pi}{2a\sqrt{Bb}}. \tag{10}$$

Once closure occurs, of course, the linear description of widening becomes irrelevant. When the number of monomers available to the domain is insufficient for the width to reach $\pi/2$, the domain is frozen in a nonspherical state. In a multidomain sample, because domains form at different times, they will grow to different sizes before they fill the available space. Since size translates into domain age, we can also say that a domain will become a spherulite above a certain size; below that size it will not.

Closure will be frustrated if the polymerization is complete before T_c. The saturation time T_s represents the end of polymerization, and can be approximated by $3t_{1/10}$, where

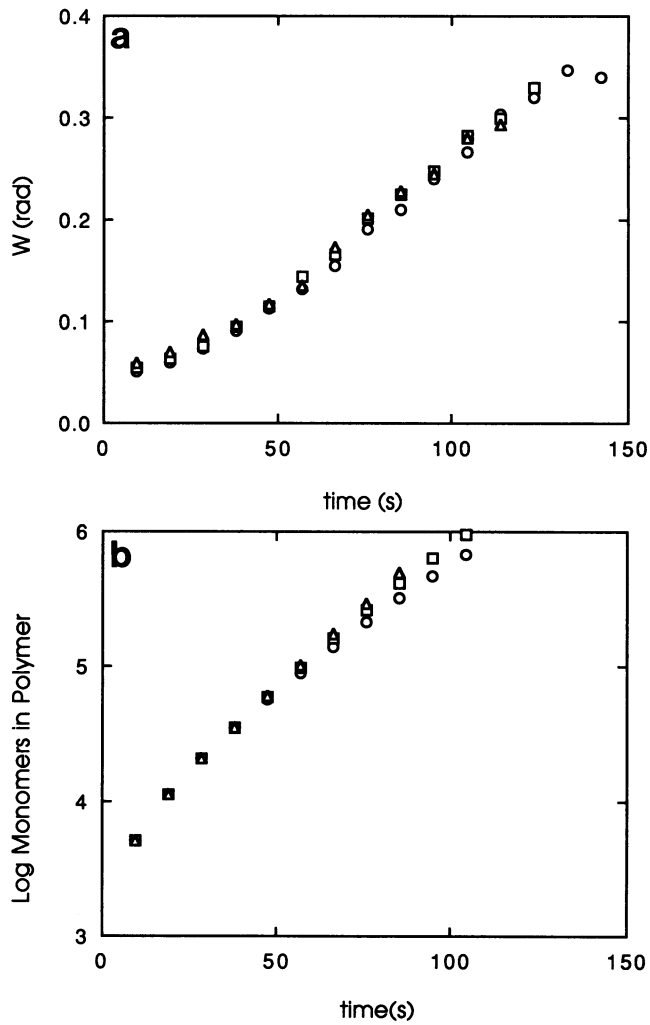

FIGURE 11 The effect of a maximum density ceiling on the simulations. (*a*) The width of the distribution as a function of time. There is no change in the rate of domain expansion when the maximum density is significantly lowered. (*b*) The total monomer concentration is shown as a function of time. It is sensitive to the lowered ceiling. The ceiling values were 3.3 and 1.65 monomers per μm^2. The grid employed was 0.5 × 0.5 μm.

$t_{1/10}$ is the time for the reaction to reach 10% of its final value. The factor of 3 is justified by observation of progress curves (Ferrone et al., 1985b). If anything, this will be an overestimate of T_s. For the range of conditions of interest, log $t_{1/10}$ is closely proportional to −log B (as seen in Fig. 12). Concentration changes can also be implicitly parametrized by the growth rate B, since B is a function of c. Thus, as concentration increases, saturation drops as −log B, while closure time drops only as −1/2 log B. This implies that the closure and saturation times will cross, as shown in Fig. 12. At small concentrations (or B values), closure is reached well before saturation, and spherulites result. At high concentrations and B values, the monomer supply is exhausted before closure.

The crossing of closure and saturation times is sensitive to the deflection (bending) rate, of course. For the range of b values used here, the two curves cross between 100 and 1000 s, (33 s $< t_{1/10} <$ 330 s) at a concentration between 24 and 25 g/dl.

In some types of experiments there is a reservoir of monomers available to the growing domain. This occurs in photolysis experiments where a single domain is formed in the laser beam, and into which monomers outside the beam can diffuse (Basak et al., 1988; Cho and Ferrone, 1990; Cho and Ferrone, 1991; Ferrone et al., 1985b; Ferrone et al., 1980; Hofrichter, 1986). In such a case, a spherulite will invariably form. However, the time for the formation is still given as shown.

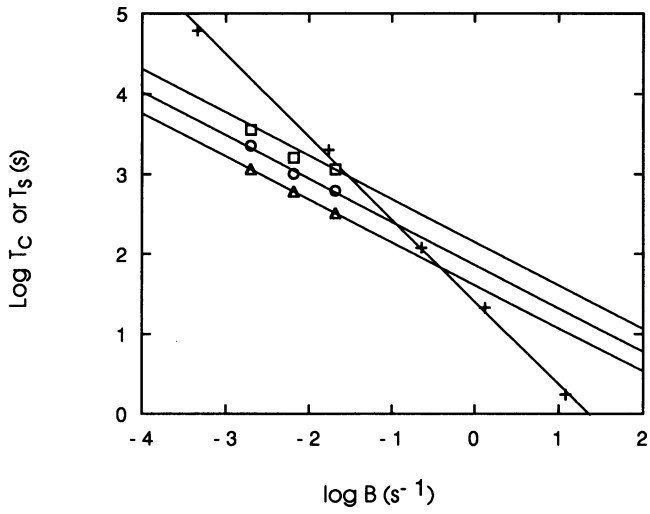

FIGURE 12 Comparison of the log of saturation time T_s (*steep line*) and closure time T_c (*group of three lines*) for different exponential growth rates, B. Exponential growth rates are highly dependent on concentration (Ferrone et al., 1980). For the range of log B shown, the concentration ranges from about 21 g/dl (at −4) to 36 g/dl (at 2). Saturation time is obtained as three times the tenth time, $t_{1/10}$, (Ferrone et al., 1985b) and is shown as the + signs. This is very nearly proportional to B^{-1}, as shown by the solid line, which is fit to the data shown by the + signs. The closure time is found from Eq. 10. The symbols show results of the simulations as nucleation rate g and deflection rate b are changed, while the lines show the relationship of Eq. 10. Points connected by a line have the same value of b. The saturation time is much more sensitive to the concentration, due to the high concentration sensitivity of the tenth time, than is the closure time. The two curves cross near 100 s, at a concentration of about 26 g/dl, implying that typical domains at $c >$ 26 g/dl will not be spherulitic. Three different values of b are drawn (b = 0.02, 0.08, and 0.32 s^{-1}). The center value is the one most closely corresponding to the data of Samuel et al. (1990).

Comparison with experiments

The most critical comparison of this model to experimental observations must be in the geometry of the growing domain, as it converts from a small, narrow sheaf to a spherulite. Domains with twofold symmetry have been observed at early reaction times in several types of experiments. White and Heagan (1970), using optical microscopy, saw distinct wheat sheaf patterns. They commented that "A few fine filaments arranged in the form of an "X" and tufts of fibers resembling bow ties were the first structures to appear."

Mizukami and-coworkers (personal communication) observed early phases of gelation by electron microscopy of sectioned cells. They found small linear structures in many different parts of the cell, while no star or radial shaped fiber arrays were seen. This again suggests that domains can begin from nearly linear polymer arrays.

The most direct comparison is provided by the time-resolved images of birefringence obtained by Basak et al. (1988) in laser photolysis experiments. The symmetry of the initial birefringence was clearly twofold, and evolved into spherical domains with time. Since only a small fraction of the sample was photolyzed, diffusion of monomers from ungelled regions allowed the reaction to proceed and spherulites invariably formed. The characteristic times for the transformation of symmetry in those experiments was in the 100–800-s range. The temperatures in those experiments were lower than those used in these simulations, so that we must adjust B for the concentration and temperature used. Taking b as unchanged, the projected time of closure is 100 s. The lower temperature is likely to lower b, improving agreement further. However, there is no information at present on the temperature dependence of the rate of polymer bending, so changes in temperature cannot be simulated quantitatively. For birefringence measurements, it is also important to realize that a substantial number of aligned polymers are required, which need not be the case at the domain closure time but may follow it.

A widely used technique for the study of sickle hemoglobin gelation is the temperature jump method, in which a solution of deoxyhemoglobin is rapidly warmed so that the solubility is exceeded and polymerization ensues. However, this method is limited by the need to maintain deoxyhemoglobin in a soluble state. A typical lower temperature limit is 4–5°C, which gives a solubility of 27 g/dl (Ross et al., 1977). Thus typical thermal induction experiments are performed below 27 g/dl, and are likely to give rise to well formed spherulites.

Photolysis studies do not have the time/concentration restriction of the thermal method. However, single domains have the infinite reservoir of monomers in the nonphotolyzed

regions available via diffusion to continue the reaction until full spherulites are formed. In photolysis experiments on single cells with *finite* volumes of hemoglobin, spherulitic domains need not form, as clearly seen in the pictures of Mozzarelli et al. (1987).

In gels produced by photolysis at high concentrations, a large number of nucleation events occur which produce a well defined mean and remove the stochastic behavior. As the tenth time is shortened, and the number of domains increases, one or two domains could be resolved, but the expected pattern of many tiny spherulites never materialized (Ferrone, unpublished observation). The explanation is now clear. The smaller domains had not formed spherulites, and even the extended growth due to diffusion could not produce the expected pattern.

Although the primary focus of this work is on the spatial aspects of the growth of domains, the simulations also probe another aspect of the modelling of sickle hemoglobin polymerization. The exponential growth of the concentration of polymerized monomers, observed by light scattering measurements, was successfully explained by the double nucleation model as first formulated (Ferrone et al., 1985a, 1985b). The model assumed that the polymers nucleated in proportion to the concentration of other polymerized monomers. This assumption equated the available surface area, on which nucleation occurs, with the total polymerized monomer concentration, effectively assuming that the polymers were dilute and separate. In replacing those simplifying assumptions by somewhat more realistic descriptions, it is seen that growth remains well described as exponential for about one and a half decades (cf. Fig. 9). In single domain experiments, this is comparable to the quality of the data (Hofrichter, 1986). Multidomain experiments show exponential growth over a larger range, but there other effects of the formation of domains will be included, and this is beyond the scope of this paper (Eaton and Hofrichter, 1990).

Extensions to three dimensions

Although this work has not been carried out in three dimensions, the consequences of these simulations can be qualitatively visualized. Higher symmetry is not expected, but in fact lower symmetry is the likely outcome. Just as the symmetry of a single straight polymer has been lowered by the curvature that results from polymer bending in two dimensions, so will a type of twist about the initial polymer axis likely occur in three dimensions. The rules regarding scaling of the distributions must continue to hold; however, the linear relationships seen in two dimensions widening of the domain must await a detailed calculation to assure their continuance in the higher dimension. For three dimensional simulations an added problem emerges, viz. comparison with data. For good optical measurements, most domains have been studied in thin slides, and so, after initial growth, are closer to two dimensions than three dimensions entities.

Physiological implications

In a physiological setting, the red cell exchanges oxygen at a finite rate, and hence the polymerization process is controlled by different features than seen in typical temperature jump or photolysis experiments. Nucleation occurs at a lower supersaturation, but with high nonideality; the growth rate will ultimately be limited by the rate of oxygen removal. A key observation of the simulations presented here is that the expected time of closure is always above 1 s. On the other hand, the cell's transit through the capillaries will be no more than 1–2 s (Sarelius and Duling, 1982). Therefore, even allowing for some precapillary exchange of O_2, it is unlikely that spherulites will form. Consequently, we would argue that typical physiological gelation involves nonspherulitic domains.

Mickols et al. (1988) studied fixed, gelled single cells using polarized absorbance. Domains were formed by dexoygenation which is somewhat more gradual than occurs in the normal physiological processes, and also proceeded to complete desaturation. Nonetheless, it allows the implications of gradual (i.e., a few seconds) deoxygenation to be examined. About 40% of the cells studied had clearly twofold forms, and about the same percentage had multiple aligned regions. The latter could either be complete domains, or multiple domains. (The remaining 20% of the cells have two or three birefringence lobes.) Thus a substantial percentage are not typical spherulites. Deoxygenation to a finite oxygen pressure, rather than to zero pO_2, would have produced even more twofold forms, since the formation of spherulites is a later occurrence. The very large percentage of nonspherulitic forms seen, therefore, supports the prediction that physiological deoxygenation is not dominated by the appearance of classic spherulites. These finding have important implications for understanding vasooclusion. A bundle of fibers will have quite different effects on a cell traversing the microcirculation than will a spherical array of the same polymer mass. Moreover, the rate of widening may set a second clock against which the cell's circulation must be measured. A transient delay in capillary passage of the order of a minute could allow spherulites to form, which would create greater complications.

This also raises the troublesome issue of the relevance of most viscosity measurements. Deoxy gels which are thermally induced, as in most viscometric studies, will create spherulites, which are not the dominant form in vivo. Bulk cellular studies may be no better if the effect of intercellular motion is dominant over the physiologically relevant internal cellular deformability.

REFERENCES

Basak, S., F. A. Ferrone, and J. T. Wang. 1988. Kinetics of Domain Formation by Sickle hemoglobin Polymers. *Biophys. J.* 54:829–843.

Beach, D. A., C. Bustamante, K. S. Wells, and K. M. Foucar. 1988. Differential polarization imaging. III. Theory confirmation. Patterns of polymerization fo hemoglobin S in red blood cells. *Biophys. J.* 53:449–456.

Brieh, R. W., E. S. Mann, and R. Josephs. 1990. Length distributions of hemoglobin S fibers. *J. Mol. Biol.* 211:693–698.

Cho, M. R., and F. A. Ferrone. 1990. Monomer diffusion into polymer domains in sickle hemoglobin. *Biophys. J.* 58:1067–1073.

Cho, M. R., and F. A. Ferrone. 1991. Monomer diffusion and polymer alignment in domains of sickle hemoglobin. *Biophys. J.* 63:205–214.

Eaton, W. A., and J. Hofrichter. 1990. Sickle cell hemoglobin polymerization. *Adv. Protein Chem.* 40:63–280.

Ferrone, F. A. 1989. Kinetic models and the pathophysiology of sickle cell disease. *Ann. N.Y. Acad. Sci.* 565:63–74.

Ferrone, F. A., J. Hofrichter, H. Sunshine, and W. A. Eaton. 1980. Kinetic studies on photolysis-induced gelation of sickle cell hemoglobin suggest a new mechanism. *Biophys. J.* 32:361–377.

Ferrone, F. A., J. Hofrichter, and W. A. Eaton. 1985a. Kinetics of sickle hemoglobin polymerization II: a double nucleation mechanism. *J. Mol. Biol.* 183:611–631.

Ferrone, F. A., J. Hofrichter, and W. A. Eaton. 1985b. Kinetics of sickle hemoglobin polymerization I: studies using temperature-jump and laser photolysis techniques. *J. Mol. Biol.* 183:591–610.

Hofrichter, J. 1986. Kinetics of sickle hemoglobin polymerization III. Nucleation rates determined from stochastic fluctuations in polymerization progress curves. *J. Mol. Biol.* 189:553–571.

Mickols, W., J. D. Corbett, M. F. Maestre, I. Tinoco, J. Kropp, and S. H. Embury. 1988. The effect of speed of deoxygenation of the precentage of aligned hemoglobin in sickle cells. Application of differential polarization microscopy. *J. Biol. Chem.* 264:4338–4346.

Mozzarelli, A., J. Hofrichter, and W. A. Eaton. 1987. Delay time of hemoglobin S polymeriztion prevents most cells from sickling. *Science (Wash. DC).* 237:500–506.

Ross, P. D., J. Hofrichter, and W. A. Eaton. 1977. Thermodynamics of gelation of sickle cell deoxyhemoglobin. *J. Mol. Biol.* 115:111–134.

Samuel, R. E., E. D. Salmon, and R. W. Briehl. 1990. Nucleation and growth of fibres and gel formation in sickle cell haemoglobin. *Nature (Lond.).* 345:833–835.

Sarelius, I. H., and B. R. Duling. 1982. Direct measurement of microvessel hematocrit, red cell flux, velocity and transit time. *Am. J. Physiol.* 243: H1018-H1026.

White, J. G., and B. Heagan. 1970. The fine structure of cell free sickled hemoglobin. *Am. J. Pathol.* 58:1–17.

Zhou, H. X., and F. A. Ferrone. 1990. Theoretical description of the spatial dependence of sickle hemoglobin polymerization. *Biophys. J.* 58: 695–703.